Non-diffusional growth mechanism of I_1basal stacking-faults inside twins in hcp metals

Andriy Ostapovets[1], Anna Serra[2] and Robert C. Pond[3]

[1]*Central European Institute of Technology - Institute of Physics of Materials (CEITEC IPM), Academy of Sciences of the Czech Republic, Žižkova 22, 61662 Brno, Czech Republic*
[2]*Department of Civil & Environmental Engineering, Universitat Politecnica de Catalunya, Jordi Girona 1-3, 08034 Barcelona, Spain*
[3]*College of Engineering, Mathematics and Physical Sciences, University of Exeter, Exeter, EX4 4QF, United Kingdom*

Abstract

Deformation twins in magnesium exhibit considerable densities of I_1 basal-plane stacking-faults. Since these faults generally transect their host twin, they presumably lengthen concommitantly with boundary migration during twin growth. We investigate this process using atomic-scale simulation for $\{10\bar{1}2\}$ and $\{10\bar{1}1\}$ twinning. It is demonstrated first that the intersection of a stacking-fault with a stationary twin boundary is delineated by a sessile imperfect disconnection. Subsequently, by applying a shear strain, we stimulate twin growth by the passage of twinning disconnections along twin boundaries, and show that these are able to propagate through such pre-existing imperfect disconnections in a conservative manner.

Recently, several researchers have reported abundant I_1 stacking-faults (SFs) inside deformation twins in magnesium alloys [1-6]. These SFs generally transect their host twins, terminating at intersections with twin boundaries (TBs). This observation implies that the SFs extended concomitantly with twin growth. Since the growth of deformation twins is a process occurring without diffusion, we infer that the associated extension of SFs is also a conservative process. By contrast, expansion or contraction of I_1 SFs in the bulk of single crystals of hcp metals does require a diffusive flux of point defects because the Frank partial dislocations bounding such faults can only move by climb [7]. Further support for the conjecture that SF growth during twinning is conservative is provided by a recent study using atomic-scale simulation [8] which found that the motion of twinning disconnections along twin boundaries – the elementary mechanism of twin growth – is not impeded by encountering SF-TB intersections. The objective of the present paper is to confirm that concomitant SF and twin growth is conservative. There are two aspects to be addressed: first, we formally characterize the defect delineating the intersection of a SF with a TB, and second, we show that motion of a twinning disconnection through such an intersection does not require diffusion. Detailed analyses of both aspects are presented for the case of $\{10\bar{1}2\}$ twinning, and a briefer treatment is outlined for $\{10\bar{1}1\}$ twinning.

Simulations were carried out using the LAMMPS software [9], with atomic forces described by the EAM potential developed by Liu et al. [10], and OVITO [11] for visualization. We used the procedure described by Sun et al. [12] and also reported by Ostapovets and Serra [13] to create a twin in our simulation block. Two twin embryos were induced to grow by application of a shear strain, and a SF arises where the

twin tips, impinge. After coalescence, twin growth continues by glide of twinning disconnections along the coherent twin boundaries [13-15].

Fig. 1 shows the detailed atomic structure of a SF-TB intersection. We distinguish A, B, and C type basal planes using red, green and blue respectively. On the left-hand side, both the parent (upper) and twin (lower) are …ABAB… crystals (red-green), while on the right-hand side, the lower crystal is …ACAC… (red-blue).The SF is clearly seen where the stacking sequence changes from …ABAB… to …ACAC… in the lower crystal. The interface structures on either side of the SF are therefore not identical, but may be virtually energetically degenerate. Whereas the bicrystal on the left of the SF is a true $(10\bar{1}2)$ compound twin, corresponding atoms in the parent (designated λ) and twin (designated, μ) on the right are not in exactly mirrored locations across the interface.

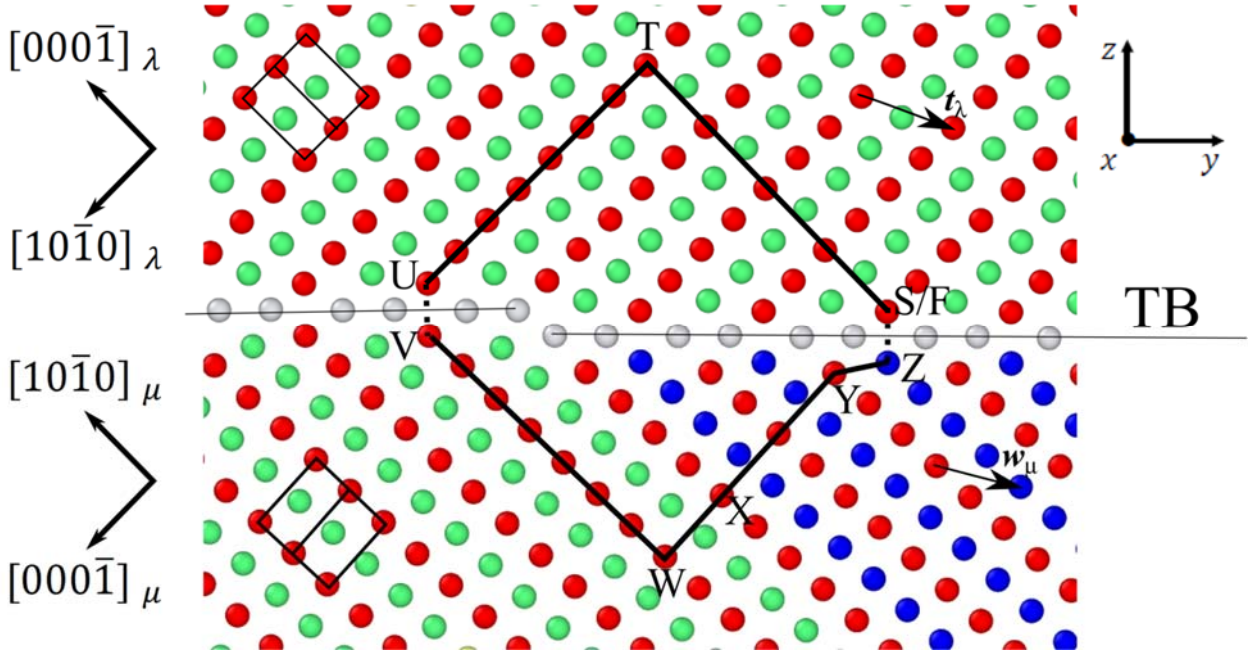

Fig. 1 Closed right-handed circuit around a SF-TB intersection in a $(10\bar{1}2)$ twin. The projection direction is $[1\bar{2}10]$, i.e. antiparallel to the defect's line direction, $\boldsymbol{\xi}$. Basal planes in A, B and C close packed positions are colored red, green and blue, respectively. The axes x, y, z are parallel to $[\bar{1}2\bar{1}0]_\mu$, $[\bar{1}011]_\mu$ and $[10\bar{1}2/\Lambda^2]_\mu$ respectively, where $\Lambda^2 = \frac{2}{3}\left(\frac{c}{a}\right)^2$.

Evidently, the twin boundary structure is perturbed at the SF-TB intersection, being delineated by an interfacial line defect and step. To establish the topological character of this defect a closed circuit is constructed around it. However, since such a circuit cannot be completed in the traditional manner using only translation vectors [7], we use the method of generalized circuit mapping [16]. To be consistent with the RH/FS convention [7], the circuit is clockwise about the defect's line direction, $\boldsymbol{\xi}$, which is "out of the page" and parallel to $[\bar{1}2\bar{1}0]_{\lambda,\mu}$, starting at the point S, which is also the finishing point F in the deformed bicrystal. The circuit depicted in Fig. 1 is comprised of the segments ST, TU, UV, VW, WX, XY, YZ and ZF, which are specified in Table 1. Since the circuit crosses the interface twice, these must be equal and opposite displacements so that they do not contribute to the closure failure, i.e. $UV = \boldsymbol{v}$ and $ZF = -\boldsymbol{v}$,.

At the A-type atomic site marked X the "observer", who is navigating the circuit, undergoes mirror reflection through the $(10\bar{1}0)_\mu$ plane, an operation which exchanges his surroundings from the red-green crystal to the red-blue one. In matrix notation, this operation is denoted $(\boldsymbol{M}_{(10\bar{1}0)_\mu}, 0)^*$, where the asterisk indicates that the operation is not a symmetry element belonging to the crystal space group. (We note that $(\boldsymbol{M}_{(10\bar{1}0)_\mu}, 0)^*$ leaves the red sites invariant and shifts green sites to blue ones, and hence, for convenience, we retain the μ coordinate frame unchanged.) The segment YZ links a red site to a blue site by the c-mirror-glide operation $(\boldsymbol{M}_{(10\bar{1}0)_\mu}, 1/6[\bar{2}023]_\mu)$.

The sequence of all the above operations defines the overall operation which transports the observer from S to F in the reference space [16]. In brief, the two mirror operations in the circuit mutually cancel, and, after further cancellation of anti-parallel translation segments, the resultant closure failure is the displacement $(\boldsymbol{I}, \boldsymbol{SF})$, where $\boldsymbol{I}$ represents the identity, thereby characterizing a dislocation with Burgers vector $\boldsymbol{FS} = \boldsymbol{b}^p$. Alternatively expressed, the irreducible description of the circuit [16] is given by

$$\boldsymbol{b}^p = \boldsymbol{t}(\lambda) - \boldsymbol{P}\boldsymbol{w}(\mu) \qquad (1),$$

where $\boldsymbol{t}(\lambda) = 1/3[\bar{2}113]_\lambda$ and $\boldsymbol{w}(\mu) = 1/6[\bar{6}243]_\mu$, as shown in Fig. 1, and $\boldsymbol{P}$ is the matrix which re-expresses μ vectors in the λ frame. For ideal c/a, $\boldsymbol{b}^p = 1/102[2,0,\bar{2},15]_\lambda$ which has a magnitude of $0.243a$. It is now helpful to introduce the Cartesian bicrystal coordinate frame x, y, z, depicted in Fig. 1. Re –expressing $\boldsymbol{b}^p$ in this frame we have $\boldsymbol{b}^p = [b_x^p, b_y^p, b_z^p]$, and the magnitudes of the components are set out in Table 2: we note that $b_z^p = -d/3$, where d represents the spacing of $(10\bar{1}2)$ lattice planes.

Circuit Element	Matrix Operation
ST	$(\boldsymbol{I}, [000\bar{4}]_\lambda)$
TU	$(\boldsymbol{I}, 1/3[10\ 1\ \overline{11}\ 0]_\lambda)$
UV	$(\boldsymbol{I}, \boldsymbol{v})$
VW	$(\boldsymbol{I}, 1/3[\overline{10}\ \bar{1}\ 11\ 0]_\mu)$
WX	$(\boldsymbol{I}, [0001]_\mu)$
X	$(\boldsymbol{M}_{(10\bar{1}0)_\mu}, 0)^*$
XY	$(\boldsymbol{I}, [0002]_\mu)$
YZ	$(\boldsymbol{M}_{(10\bar{1}0)_\mu}, 1/6[\bar{2}023]_\mu)$
ZF	$(\boldsymbol{I}, -\boldsymbol{v})$

Table 1. Elements of the circuit SF around a SF-TB intersection in a $(10\bar{1}2)_{\lambda,\mu}$ twin boundary. The symbol $\boldsymbol{I}$ represents the identity operation.

The SF-TB defect also exhibits step character, which we characterize following the method of Hirth and Pond [17]. The overlap step height is defined as the smaller of the free surface steps on the λ and μ surfaces before bonding to create the bicrystal. These are equal to $\boldsymbol{n}\cdot\boldsymbol{t}(\lambda)=d$ and $\boldsymbol{n}\cdot\boldsymbol{w}(\mu)=\frac{2}{3}d$ respectively, so the latter defines the overlap step height, h^p. Thus the SF-TB intersection is an imperfect disconnection, $(\boldsymbol{b}^p, h^p)$.

$\boldsymbol{b}$	$b_x\,(a)$	$b_y\,(a)$	$b_z\,(a)$	$h\,(d)$
$\boldsymbol{b}^p=\frac{1}{102}[2,0,\bar{2},15]_\lambda$	0	0.140	−0.198	$\frac{2}{3}$
$\boldsymbol{b}^t=\frac{1}{17}[10\bar{1}\bar{1}]_\lambda$	0	−0.140	0	2
$\boldsymbol{\delta}^{SF}=[10\bar{1}0]_\mu$	0	−1.260	1.188	-

Table 2. Topological character of defects and SF displacement vector ($\boldsymbol{\delta}^{SF}$) in the $(10\bar{1}2)$ twin boundary. Indices are given for the case of ideal $\frac{c}{a}$.

Fig. 2 shows a pair of snapshots as a twinning disconnection, $\left(\boldsymbol{b}^t, h^t\right)$, glides from left to right along a $(10\bar{1}2)_{\lambda,\mu}$ TB, encountering and passing through a SF-TB disconnection, $(\boldsymbol{b}^p, h^p)$. Twinning disconnections in $(10\bar{1}2)_{\lambda,\mu}$ TBs have been investigated previously [14] and shown to have $\boldsymbol{b}^t=\frac{1}{17}[10\bar{1}\bar{1}]_\lambda$ and $h^t=2d$ for ideal $\frac{c}{a}$: the components are listed in Table 2, and we note that $b_y^t=-b_y^p$.

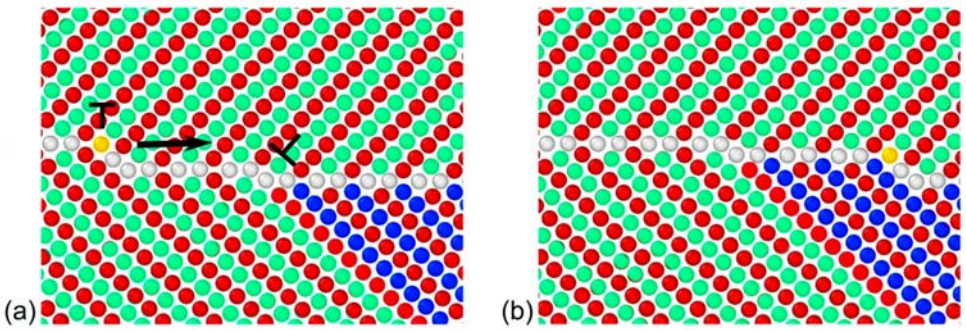

Fig. 2. Sequence of simulations showing the migration of a $(10\bar{1}2)$ twin boundary by glide of a twinning disconnection and the consequent extension of a SF. An atom in the core of the twinning disconnection is indicated as a yellow marker. The projection direction is $[1\bar{2}10]$.

To assess any diffusional flux accompanying this interaction, we follow the analysis of Hirth and Pond [17] in which the dislocation and step components of disconnections are treated separately. The Burgers vector components and step heights are depicted schematically in Fig. 3. Since the Burgers vector of the twinning disconnection has the form $\boldsymbol{b}^t=[0,b_y^t,0]$, motion parallel to x or y would not

require any flux, but motion parallel to z would. In the course of interaction, the twinning disconnection must climb down the step of the imperfect defect: this would require $\left(b_y^t h^p\right)X$ atoms per unit length of defect to diffuse away, where X is the number of atoms per unit volume in hcp crystals. For the imperfect defect, $\boldsymbol{b}^p = [0, b_y^p, b_z^p]$, so flux contributions would be required for motion parallel to y or z. The latter corresponds to climb up the step of the twinning disconnection, so requires $\left(b_y^p h^t\right)X$ atoms per unit length of defect to diffuse away. Motion of the imperfect defect parallel to y arises on two accounts: first, the SF extends by $[10\bar{1}0]_\mu$ which includes a component parallel to y equal to $\delta_y^{SF} = -\sqrt{3}\,a\cos\left(tan^{-1}\frac{c}{a\sqrt{3}}\right)$, and, second, passage of the twinning disconnection reduces this displacement by b_y^t. Thus, the flux required is $b_z^p\left(\delta_y^{SF} - b_y^t\right)X$ atoms per unit length of defect to diffuse towards the defect, and hence the total number of atoms, δN is equal to

$$\delta N = \left\{-b_y^t h^p - b_y^p h^t + b_z^p\left(\delta_y^{SF} - b_y^t\right)\right\}X \qquad (2),$$

where +/- signs signify flux toward/away from the defects. The three terms inside the bracket of equation (2) can now be computed, as listed in Table 3, where the quantities are specified in units of ad. Since their sum gives $\delta N = 0$, the interaction is conservative, and the interaction is described as involving compensated climb. One can readily show that this result is independent of the $\frac{c}{a}$ ratio, and whether twinning or de-twinning is occurring.

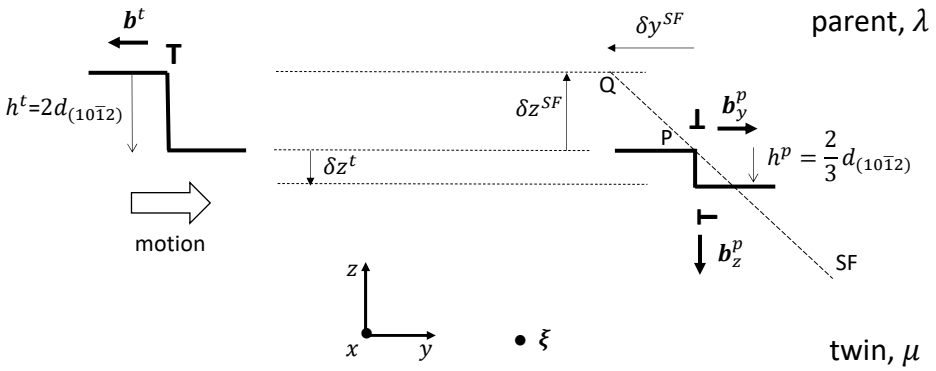

Fig. 3. Schematic illustration of a twinning disconnection approaching a SF-TB intersection in a $(10\bar{1}2)$ twin boundary. The Burgers vectors and step heights of the disconnections are indicated. The extension of the SF is $PQ = [10\bar{1}0]_\mu$, and the lateral displacement of the SF-TB defect is the horizontal component of PQ reduced by b_y^t following passage of the twinning disconnection.

Flux terms in Equ. (2)	Magnitude (ad)
$-b_y^t h^p = -b_y^t \frac{2d}{3}$	-0.093
$-b_y^p h^t = -b_y^p 2d$	-0.280
$b_z^p\ \delta y^p = \frac{d}{3}(\delta_y^{SF} - b_y^t)$	0.373
total	0

Table 3. Flux contributions for passage of a twinning disconnection through a SF-TB intersection in a $(10\bar{1}2)$ twin boundary. The units of the magnitudes are *ad* where *a* is the lattice parameter and *d* is the interplanar distance.

The concomitant extension of I_1 SFs with the growth of $(10\bar{1}1)$ twins in a conservative manner is similar to the $(10\bar{1}2)$ case discussed above. SF intersections with $(10\bar{1}1)$ twins have been studied previously using atomic-scale simulation [8], and an example is illustrated in Fig. 4. Here we analyse the intersection using the topological method [16]. Substituting $\boldsymbol{t}(\lambda) = [0001]_\lambda$ and $\boldsymbol{w}(\mu) = 1/6[\bar{4}043]_\mu$ into equation (1), we obtain for ideal c/a, $\boldsymbol{b}^p = 1/246[4,0,\bar{4},33]_\lambda$ which has a magnitude of $0.221a$, and components listed in Table 4. The defect also exhibits an overlap step height, $h^p = 5d/6$ (where d now represents the spacing of the $(10\bar{1}1)$ lattice planes), i.e. the smaller of $\boldsymbol{n}\cdot\boldsymbol{t}(\lambda) = d$ and $\boldsymbol{n}\cdot\boldsymbol{w}(\mu) = 5d/6$. Thus, this SF-TB intersection is also delineated by a sessile, imperfect disconnection.

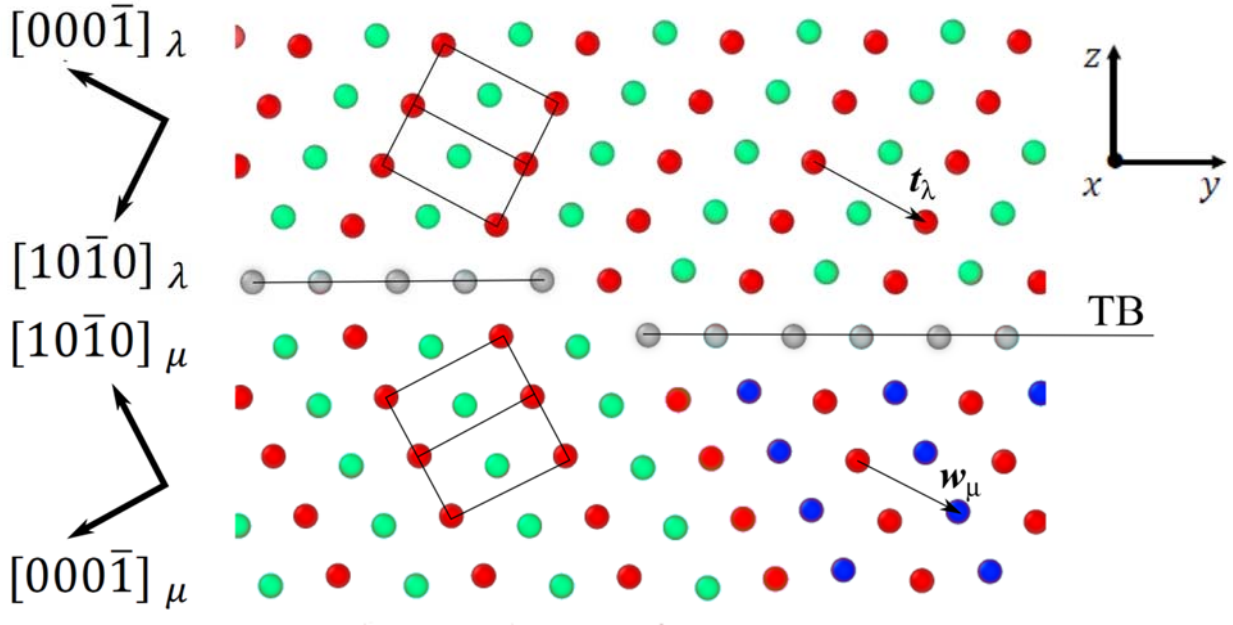

Fig. 4 A SF-TB intersection in a$(10\bar{1}1)$ twin. The projection direction is $[1\bar{2}10]$. The axes x, y, z are parallel to $[\bar{1}2\bar{1}0]_\mu$, $[\bar{1}012]_\mu$ and $[10\bar{1}1/\Lambda^2]_\mu$ respectively, where $\Lambda^2 = \frac{2}{3}\left(\frac{c}{a}\right)^2$.

We consider $(10\bar{1}1)$ twin growth to occur by passage of disconnections $(\boldsymbol{b}^t, h^t)$, where $\boldsymbol{b}^t = \frac{1}{246}[22\ \overline{82}\ 60\ \bar{3}]_\lambda$ and $h^t = 2d$ [8, 14,18], as listed in Table 4, and which has been observed experimentally in Ti [19]. Evidently, $\boldsymbol{b}^t$ has a finite component, b_x^t: however, it was proposed that twinning is accomplished by sequential glide of disconnections with opposite sign b_x^t components, so the macroscopic shearing direction is $[\bar{1}012]_{\lambda\mu}$ [14]. Moreover, b_x^t corresponds to a screw component of the twinning disconnection when $\boldsymbol{\xi}$ is parallel to $[\bar{1}2\bar{1}0]_{\lambda,\mu}$, so does not require a diffusional flux for motion in the y or z directions. We note that the sign of b_y^t is positive, i.e. opposite to that for the previous case, so climb of $(\boldsymbol{b}^t, h^t)$ down h^p requires a positive material flux. In addition, δ_y^p is equal to the component of the SF extension parallel to the interface, $\delta_y^{SF} = \frac{3\sqrt{3}a}{\sqrt{41}}$, supplemented by b_y^t since passage of the twinning disconnection offsets the lower crystal by this amount. The flux contributions associated with passage of the twinning disconnection through the SF-TB intersection are listed in Table 5. Since these sum to give $\delta N = 0$, the passage of twinning disconnections through this SF-TB intersection is conservative, as for the previous case.

$\boldsymbol{b}$	$b_x\ (a)$	$b_y\ (a)$	$b_z\ (a)$	$h\ (d)$
$\boldsymbol{b}^p = \frac{1}{246}[4,0,\bar{4},33]_\lambda$	0	0.180	-0.128	$\frac{5}{6}$
$\boldsymbol{b}^t = \frac{1}{246}[22\ \overline{82}\ 60\ \bar{3}]_\lambda$	0.500	0.225	0	2
$\boldsymbol{\delta}^{SF} = [10\bar{1}0]_\mu$	0	-0.812	1.530	-

Table 4. Topological character of defects and SF displacement vector in the $(10\bar{1}1)$ twin boundary. Indices are given for case of ideal $\frac{c}{a}$.

Flux terms in Equ. (2)	Magnitude (ad)
$b_y^t h^p = b_y^t \frac{5d}{6}$	0.187
$-b_y^p\ h^t = -b_y^p 2d$	-0.360
$b_z^p\ \delta y^p = \frac{d}{6}(\delta_y^{SF} + b_y^t)$	0.173
total	0

Table 5. Flux contributions for passage of a twinning disconnection through a SF-TB intersection in a $(10\bar{1}1)$ twin boundary. The units of the magnitudes are *ad* where *a* is the lattice parameter and *d* is the interplanar distance.

Growth of $(10\bar{1}1)$ twins can also be accomplished by disconnections with step height equal to $4d$, though they are probably less mobile than those with $h^t = 2d$ [14]. Their Burgers vectors have no component parallel to x or z, and the component parallel to y is twice that for the $2d$ defect. Thus, for considerations of diffusional flux, passage of one $4d$ twinning disconnection is equivalent to passage of two $2d$ disconnections, and is hence conservative.

In summary, we have identified the defects which delineate the intersections of I_1 SFs with $(10\bar{1}1)$ and $(10\bar{1}2)$ twins as sessile imperfect disconnections separating regions of twin interface which are virtually degenerate energetically. Furthermore, we have demonstrated that twinning disconnections can move through such SF-TB intersection defects in a conservative manner. These conclusions are consistent with the experimental observation that abundant SFs are often found in deformation twins in hcp metals, and that the SFs extend concomitantly with twin growth.

Acknowledgements
The financial supports from the Czech Science Foundation (Project 18-07140S), the Spanish MINECO (FIS2015-69017-P), and the Ministry of Education, Youth and Sports of the Czech Republic under Project CEITEC 2020 (LQ1601) are gratefully acknowledged.

References

[1] X. Zhang, B. Li, Q. Liu, Acta Mater. 90 (2015) 140-150.
[2] H. Yu, Q. Dong, Z. Yao, M.R. Daymond, Scripta Mater. 141(2017) 72-75.
[3] R. Namakian and G. Z. Voyiadjis, Acta Mater. 150 (2018) 381-393.
[4]F.L.Wang,S.R.Agnew,Int.J.Plast.81(2016)63–86.
[5]Q. Sun,X. Zhang, Y. Shu,L. Tan,Q. Liu, Mater. Lett. 185(2016)355–358.
[6] Q. Sun, Q. Zhang, B. Li, X. Zhang, L. Tan, Q. Liu, Scripta Mater. 141 (2017) 85-88.
[7] P.M. Anderson, J.P. Hirth, J. Lothe, The theory of dislocations, 3rd ed. Cambridge University Press, Cambridge, 2017.
[8] A. Ostapovets, A. Serra, J. Mater. Sci. 52 (2017), 533-540.
[9] S. Plimpton, J Comp Phys 117 (1995) 1–19.
[10] X.Y. Liu, J. B. Adams, F. Ercolessi, and J. A. Moriarty, Modell. Simul. Mater. Sci. Eng. 4 (1996) 293-303.
[11] A. Stukowski, Modelling Simul. Mater. Sci. Eng.18 (2010) 015012.
[12] Q. Sun, A. Ostapovets, X. Zhang, L. Tan, Q. Liu, Phil. Mag. 98 (9), 741-751.
[13] A Ostapovets, A Serra, Phil. Mag. 94 (2014) 2827-2839.
[14] A. Serra, R.C. Pond and D.J. Bacon, Acta Metall. Mater. 39 (1991) 1469-1480.
[15]A. Ostapovets, R. Gröger, Modell. Simul. Mater. Sci. Eng. 22 (2014) 025015.
[16] R.C. Pond, Interface Science 2 (1995) 299-310.
[17] J.P. Hirth, R.C. Pond, Acta Mater 44 (1996) 4749-4763.
[18] J. Wang, I.J. Beyerlein, J.P. Hirth, C.N. Tome, Acta Mater. 59 (2011) 3990–4001.
[19] Z. Kou, Y. Yang, B. Huang, X. Luo, P. Li, G. Zhao, W. Zhang, Scripta Mater., 139 (2017) 139-143.